ORIGINAL RESEARCH **Open access**

Influence of Spatial Resolution and Resampling on Object-Based Classification of Wetland Vegetation from UAV Imagery

Carlos Ramirez[1*], Elena Torres[2], Pablo Ortega[1], Sofia Mendes[3]

Abstract

Classifying vegetation species and ground objects using remote sensing imagery poses notable challenges, primarily due to the rich diversity of wetland plants and the extensive fragmentation of surface features. Classification of such images largely depends on spatial resolution, which plays a decisive role in determining the accuracy of both vegetation types and ground features. Despite this, further research is needed to investigate how spatial resolution and resampling procedures influence final classification outcomes. This paper focused on the core area of Huixian Karst National Wetland Park located in Guilin, Guangxi, China. Aerial images (Am) at varying spatial resolutions were captured via a UAV platform, whereas resampled images (An) at corresponding resolutions were created using pixel aggregation techniques. To analyze the effects of spatial resolution and resampling on classification performance, both the Am and An datasets were used to identify vegetation species and ground objects using geographic object-based image analysis (GEOBIA) combined with multiple machine learning classifiers. Key findings revealed that: (1) Across multi-scale imagery, the ideal scale parameter (SP) and overall processing duration both declined with coarser spatial resolution in the multi-resolution segmentation stage. At identical resolutions, the SP value for An exceeded that of Am. (2) Suitable feature variables differed between Am and An, with spectral and texture characteristics proving more influential in An compared to Am. (3) Classification outcomes from various classifiers displayed comparable patterns for Am and An across spatial resolutions from 1.2 to 5.9 cm, with overall accuracy rising initially before falling as resolution decreased. Furthermore, Am consistently achieved superior accuracy relative to An. (4) Classification accuracy for vegetation species and ground objects showed notable differences between Am and An when examined across varying spatial scales.

Keywords UAV, GEOBIA, Spatial scale, Aerial images, Resampled images, Machine learning classifier

*Correspondence:
Carlos Ramirez
carlos.ramirez@ub.edu
[1] Department of AI for Strawberry and Raspberry Greenhouse Pollination, Faculty of Agriculture, University of Barcelona, Barcelona, Spain
[2] Department of Machine Learning for Brix and Acid Levels in Citrus, Faculty of Agriculture, University of Lisbon, Lisbon, Portugal
[3] Department of Smart Pollinator Monitoring, Faculty of Agriculture, University of Porto, Porto, Portugal

Introduction

Wetlands function as transitional areas linking land and water ecosystems and rank among the three primary ecological systems alongside forests and oceans [1]. They deliver essential services including water retention, purification, flood mitigation, drought prevention, and biodiversity safeguarding. Over the last 50 years, intense human interventions have caused considerable damage to wetland ecosystems [2], as many wetlands have been repurposed for agriculture, aquaculture, and urban development, leading to sharp declines in total wetland coverage [3, 4]. Additionally, the spread of

This is an open access article distributed under the terms of the Creative Commons Attribution-NonCommercial-ShareAlike 4.0 International License (CC BY-NC-SA 4.0), which permits non-commercial use, distribution, reproduction, and adaptation in any medium or format, provided that appropriate credit is given to the original author(s) and source, a link to the license is provided, and any changes made are indicated. Adapted material must be distributed under the same license.

© 2025 The Author(s). | Published by Agro Intelligence Research Press

farmland and fishponds has led to substantial pollution of wetlands through river systems and underground water flows, threatening species diversity and damaging native habitats [5]. Currently, up to 57% of global wetlands have been lost or altered, with Asia recording the most severe reductions [6]. Hence, gaining precise insights into the spatial patterns and transformation trends of wetland vegetation species and ground objects is crucial for effective resource evaluation and utilization, while also supplying foundational data for vegetation recovery efforts and investigations into local biodiversity dynamics and underlying processes [7, 8].

Satellite remote sensing is a core technology for monitoring regional ecological conditions and is commonly used for wetland information extraction, change detection, and resource assessment [9]. Researchers have conducted extensive wetland classification using satellite datasets such as MODIS [10], WorldView-2 [11], and ALOS PALSAR [12]. However, due to limitations in spectral and spatial detail, these efforts have mainly focused on broad vegetation communities or dominant land cover categories. Significant challenges persist in distinguishing individual wetland vegetation species, which complicates the precise management and evaluation of wetland zones.

Thanks to the swift progress and increasing accessibility of unmanned aerial vehicles (UAV) in recent years, enhanced technical capabilities now support detailed ecological monitoring and assessment [13, 14]. UAV platforms offer advantages such as affordability, ease of use, and reduced reliance on specific takeoff locations or favorable weather [15]. They also enable the collection of multi-angle, high-resolution imagery tailored to user specifications, overcoming many constraints associated with traditional satellite data [16-18]. That said, image spatial resolution substantially affects outcomes in UAV applications, such as estimating fractional vegetation cover [19], recognizing plant species [20], and identifying diseases [21], among others. Changes in resolution alter how information is represented, thereby producing spatial-scale effects on analysis results. The standard approach in contemporary spatial scale research involves generating varied resolutions through resampling. Scholars have simulated UAV flights at different altitudes using methods such as pixel aggregation and cubic interpolation to examine the impact of resolution on classification accuracy. Results indicated that resolution effects on accuracy are related to mixed-pixel issues and the inherent limitations of per-pixel approaches [22]. Coarser resolutions increased pixel mixing.

Nevertheless, higher UAV image resolution does not always yield better results [23]. Raising the resolution can increase costs and complexity without guaranteeing improved accuracy. In cases of extremely fine resolution, additional details (e.g., shadows and gaps) may be recorded, complicating the image and lowering classification performance [24]. Moreover, ultra-high resolution imagery amplifies intra-class spectral and texture variations while reducing inter-class differences, hindering the identification of distinctive features for modeling [25]. Recent work, therefore, emphasizes achieving an effective balance between resolution and feature richness for reliable vegetation and ground-object identification. Still, relying exclusively on resampled imagery introduces uncertainties into spatial-scale analysis, which can compromise evaluations of classification accuracy for wetland vegetation and surface features.

Accuracy in classifying vegetation species and ground objects depends heavily on both the source imagery and the analytical methods used. Existing approaches for remote sensing classification fall mainly into pixel-based and object-based categories. Pixel-based techniques derive land cover information from single pixels or neighboring groups. Yet they overlook spatial context and texture, often resulting in a “pepper and salt” effect in very high-resolution scenes [26, 27]. In contrast, geographic object-based image analysis (GEOBIA) groups adjacent pixels sharing semantic meaning into coherent objects that incorporate spectral, textural, positional, and geometric attributes. Classification rules are then developed from these object features for information extraction [28]. Prior studies confirm that object-based techniques generally outperform pixel-based techniques in terms of accuracy [29, 30]. Given the diversity of wetland vegetation and fragmented ground features, object-based machine learning methods rank among the strongest options for wetland classification. Even so, most current research centers on comparing different algorithms, with limited examination of how they perform across varying image spatial resolutions.

To tackle these challenges, the present study collected aerial images (Am) and generated resampled images (An) at multiple spatial resolutions using a UAV platform. Wetland vegetation species and ground objects were then classified

© 2025 The Author(s). | Published by Agro Intelligence Research Press

using GEOBIA integrated with four machine learning classifiers (random forest (RF), support vector machine (SVM), K-nearest neighbors (KNN), and Naive Bayes) applied separately to Am and An. The primary goals included: (1) identifying optimal segmentation scale parameters for Am and An under different spatial scales; (2) analyzing how feature variables change across image types; (3) uncovering the scale-dependent effects of Am and An on wetland vegetation and ground object classification; (4) establishing the most suitable spatial resolution for accurately distinguishing various wetland vegetation species and ground objects.

Materials and Methods

Study area

The Huixian Wetland is located in Huixian Town, Lingui District, Guilin City, Guangxi Zhuang Autonomous Region, China. Its coordinates span 25°01′30″ N to 25°11′15″ N and 110°08′15″ E to 110°18′00″ E. Extending about 6 km in the east-west direction and 2.8 km north to south, it occupies 4.936 km². This location has a subtropical monsoon climate marked by 1894 mm of average annual rainfall and a mean yearly temperature of 19.2 °C. Shrubs and grasses form the main plant types [31]. Typical karst peak forest plain topography defines the Huixian Wetland, featuring mostly level ground. Recognized as China's biggest karst wetland system, it links the Lijiang River with the Luoqing River, serves as a safeguard for the delicate karst groundwater setting, and earns the nickname "kidneys of the Li River". The State Forestry Administration of China granted it the title Guangxi Guilin Huixian Karst National Wetland Park in 2012, highlighting its strong tourism potential, historical and cultural depth, and varied landscape [32].

Recent times have seen a major reduction in the Huixian wetland's size, alongside significant harm to biodiversity caused by nearby residents' actions and the encroachment of invasive plants (including water hyacinth and Ampullaria gigas). Thus, specific protection steps and oversight remain necessary [5]. With limited human presence, the core zone of the Huixian wetland maintains an intact ecological picture and holds key value for examining and safeguarding the Huixian karst wetland. This core zone was selected as the study area **(Figure 1)** and measures 77,398 m².

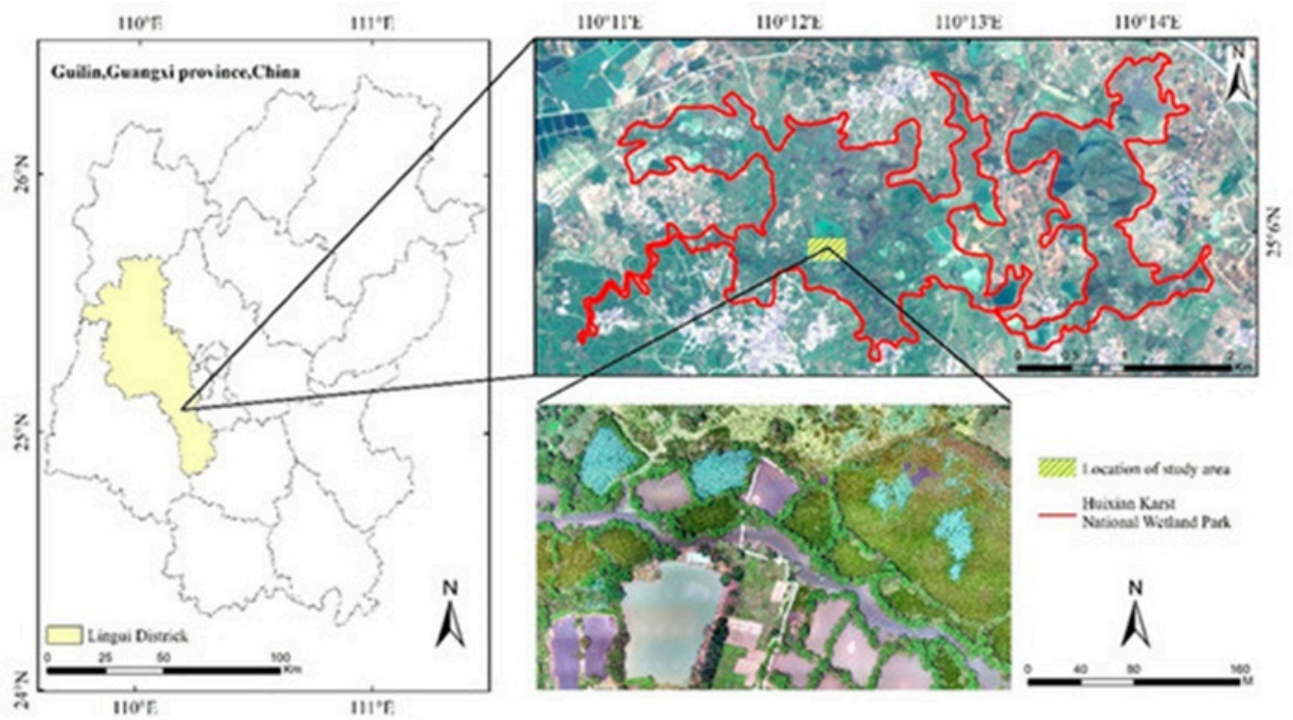

Figure 1. Overview of the study area.

© 2025 The Author(s). | Published by Agro Intelligence Research Press

Data source and preprocessing

Acquisition of field survey and UAV aerial images

Collection of the UAV aerial images took place on 1 July 2021 during peak vegetation growth in the Huixian wetland, under sunny skies and still air. A DJI Phantom 4 Pro (DJI, Shenzhen, China) served as the platform, complete with an OcuSync transmission system and a 1-inch CMOS sensor delivering 20 million effective pixels, weighing around 1.4 kg [33]. Planning and live oversight of the flight used a tablet with DJI GS Pro software, ensuring 80% forward and 70% lateral overlap while shooting straight downward at 7 m/s. Flights were conducted at elevations of 40, 60, 80, 100, 120, 140, 160, 180, and 200 m to capture RGB images at multiple spatial resolutions **(Table 1)**. Local officials granted clearance for the operation.

Table 1. The spatial resolution and the number of aerial images depend on the UAV's flight height.

Height/m	200	180	160	140	120	100	80	60	40
Resolution/cm	5.9	5.3	4.7	4.1	3.6	2.9	2.4	1.8	1.2
Aerial image/piece	25	35	48	52	76	110	159	293	640

UAV aerial image processing

POS details, including longitude, latitude, and flight posture, were first entered into Pix4D Mapper 4.4.12 software from the UAV images. Quality screening then removed unclear shots that fell below 80% heading overlap or 70% side overlap. Ground control points helped fix geometric inaccuracies and improve optimization. Automatic matching via spatial triad calculations and block adjustment followed, yielding dense point cloud information. This data supported the construction of a TIN triangulation network to produce digital orthophoto maps (DOMs).

Seamless Mosaic functionality in ENVI 5.3 handled DOM assembly and histogram equalization to achieve a uniform appearance. Cropping in ArcGIS 10.6 produced nine aerial images (spatial resolutions: 1.2, 1.8, 2.4, 2.9, 3.6, 4.1, 4.7, 5.3, and 5.9 cm). The current work used the sharpest image (1.2 cm) as the source for resampling to contrast wetland vegetation species and ground object detection between native aerial versions and processed ones. Past findings noted that nearest-neighbor, bilinear, and cubic convolution resampling introduce strong smoothing or sharpening effects that can skew outcomes [23]. Hence, pixel aggregation reduced spatial resolution and produced eight matching resampled images (spatial resolutions: 1.8, 2.4, 2.9, 3.6, 4.1, 4.7, 5.3, and 5.9 cm).

Reference data

Combining the 1.2 cm-resolution image with field-check results and photo records enabled the creation of an exact reference map showing the true vegetation species and ground objects **(Figure 2)** for validation. Areas occupied by individual vegetation categories and ground features within the study zone were also measured **(Table 2)**.

© 2025 The Author(s). | Published by Agro Intelligence Research Press

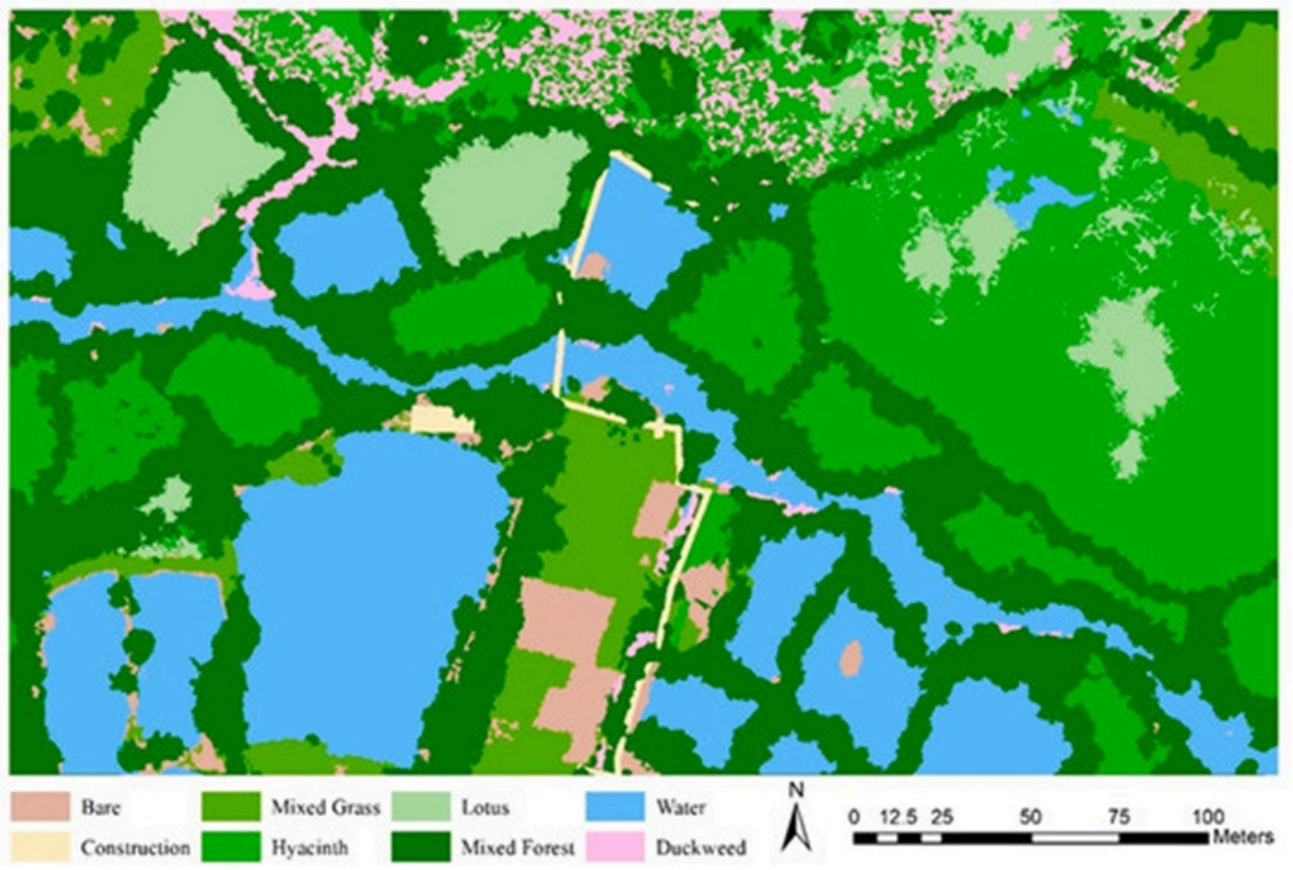

Figure 2. Ground truth reference image.

Table 2. The acreage occupied by each vegetation species and ground object in the study area.

Type	Total	Construction	Water	Bare	Mixed grass	Mixed forest	Duckweed	Hyacinth	Lotus
Acreage/m^2	77,398	511	15,839	2008	5565	24,914	2746	20,360	5455

Methods

GEOBIA processed both Am and An to sort wetland vegetation species and ground objects across the study area **(Figure 3)**. Steps included (1) choosing fitting scale parameters for multi-resolution segmentation with the ESP2 tool; (2) picking and testing feature variables via the feature space optimization function in eCognition Developer 9.0 software together with RF's mean decreased accuracy (MDA) technique; (3) running classifications on vegetation species and ground objects from multi-scale images through four machine learning classifiers (RF, SVM, KNN, Bayes); (4) judging result quality via overall accuracy, Kappa coefficient, producer accuracy, user accuracy, and average accuracy.

© 2025 The Author(s). | Published by Agro Intelligence Research Press

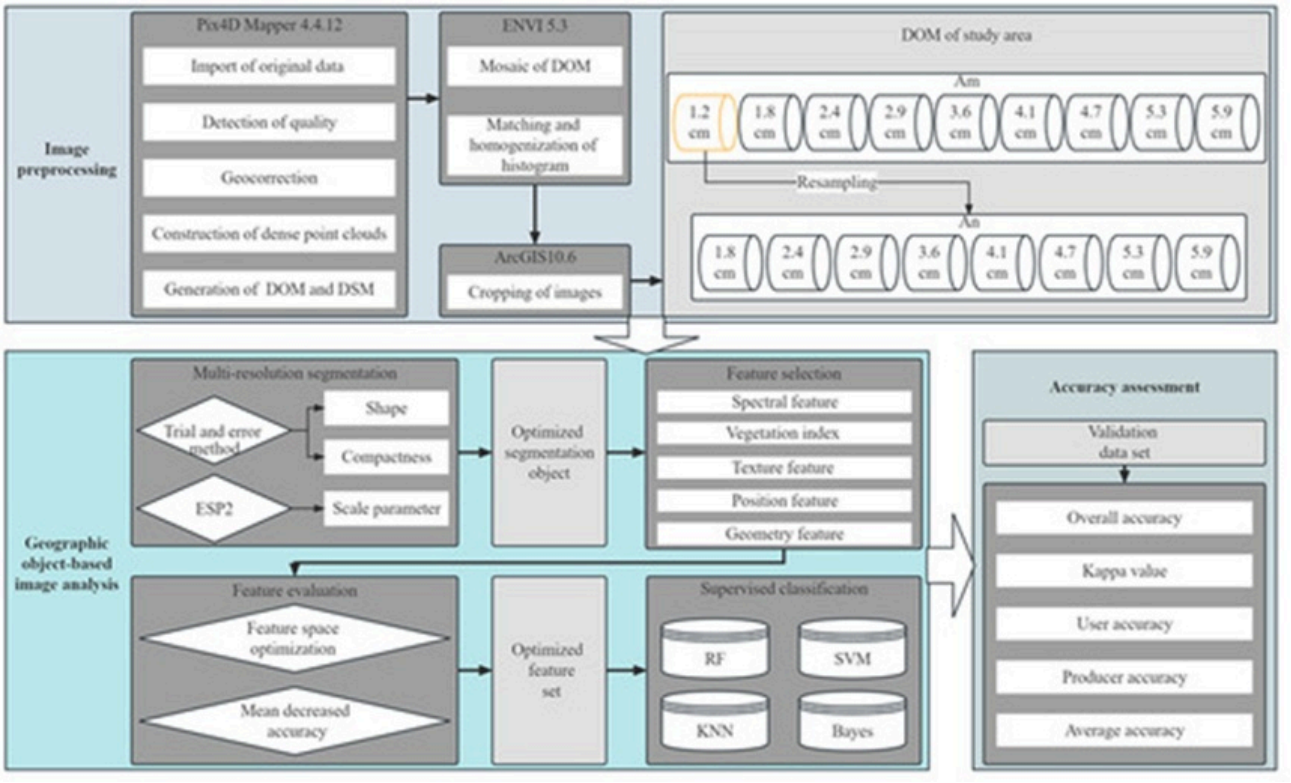

Figure 3. Technical route of this study.

Preparation of training samples

UAV photography at 40 m altitude delivered a spatial resolution of 1.2 cm, enabling straightforward visual separation of all vegetation species and ground objects. Field survey findings, combined with UAV image trait variations, led to splitting the study area vegetation into lotus, hyacinth, duckweed, mixed forest, and mixed grass groups, with ground objects placed into construction, water, and bare categories. Training samples were generated from 103 randomly placed points in ArcGIS 10.6 over the 1.2 cm image layers within the full study area **(Figure 4)**, each assigned a label **(Table 3)**.

© 2025 The Author(s). | Published by Agro Intelligence Research Press

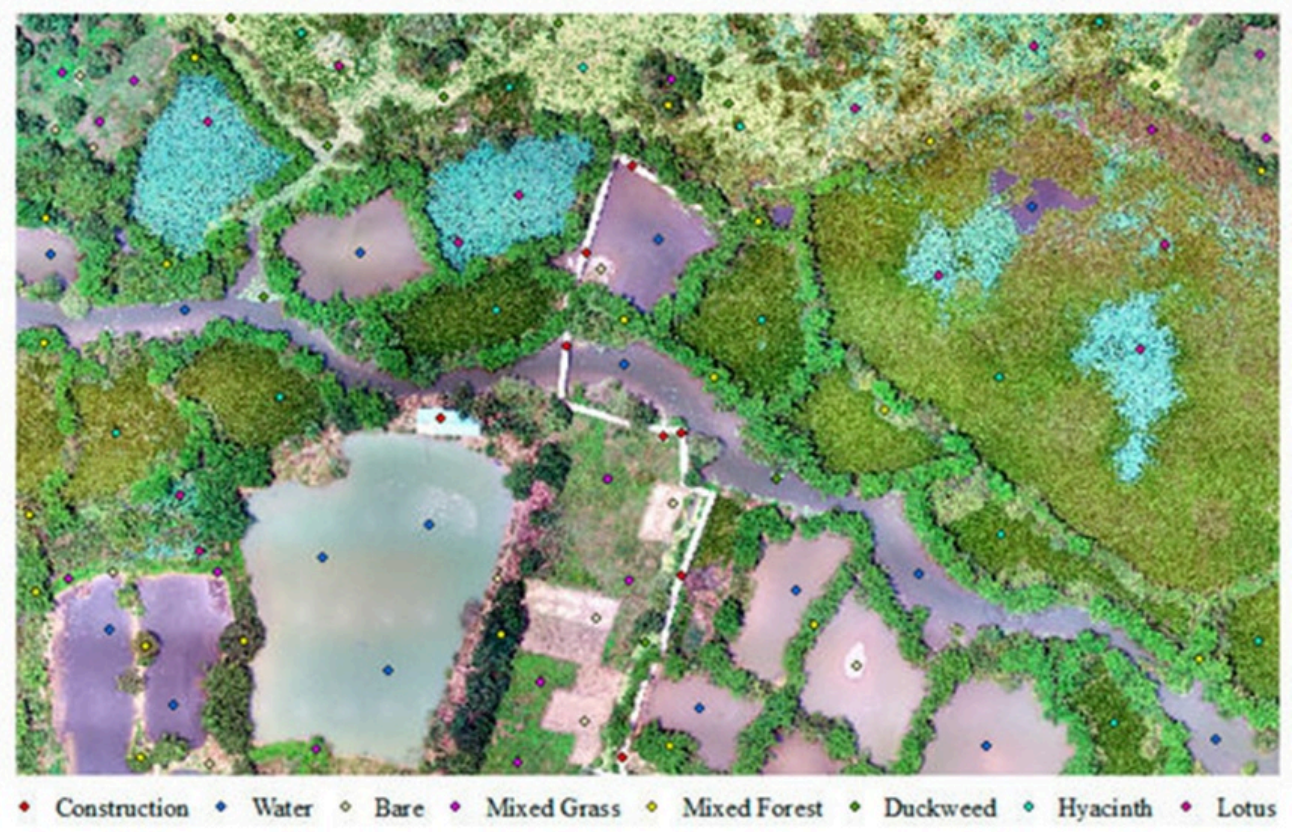

Figure 4. Spatial distribution of training samples.

Table 3. Training sample size in the study area.

Type	Total	Construction	Water	Bare	Mixed grass	Mixed forest	Duckweed	Hyacinth	Lotus
Samples size	103	8	16	11	14	20	10	13	11

Multi-resolution segmentation

GEOBIA relies mainly on image segmentation [34]. This research applied the fractal net evolution approach (FNEA) to segment both the Am and the An. The technique forms part of a multi-resolution segmentation process that combines pixels from the bottom upward according to the lowest heterogeneity level, creating objects of varying dimensions. The resulting image objects are closely aligned with the actual edges of vegetation species and ground objects, with each object containing spectral, geometric, textural, and positional details.

Within the multi-resolution segmentation process, the shape parameter measures the proportion of shape consistency relative to spectral information, while the compactness parameter functions as a component of shape to refine object compactness. The combined weights of color and shape, along with smoothness and compactness, equal 1 [35]. In eCognition Developer 9.0, users manually adjust the shape and compactness parameters, after which color and smoothness values are computed automatically.

Drawing on earlier research and additional testing, the final settings for the shape and compactness parameters were set to 0.2 and 0.5, respectively. The scale parameter (SP) regulates the internal heterogeneity of identified objects and directly affects their mean dimensions; specifically, greater SP values increase internal heterogeneity and increase pixel counts per object, whereas smaller SP values have the opposite effect. Because SP is the core element in multi-

© 2025 The Author(s). | Published by Agro Intelligence Research Press

resolution segmentation algorithms and exerts the greatest influence on classification accuracy, selecting the proper SP size is of great importance. Conventional SP determination relies on trial-and-error, a subjective and lengthy procedure [36]. Here, the ESP2 tool [37] helped establish the best SP for multi-resolution segmentation. As the starting value and increment in the ESP2 tool stayed unchanged, outcomes did not hit a maximum but instead produced a gradual or sharp curve. Hence, adjusting the initial value and step size within ESP2 proved necessary. **Table 4** lists the exact parameters finalized after repeated trials.

Table 4. Parameters of the ESP2 tool.

Parameters	Rough scale	Medium scale	Fine scale
Initial value	34	23	13
Step size	40	20	5
Number of loops	100	100	100
Shape	0.2	0.2	0.2
Compactness	0.5	0.5	0.5

Feature selection and evaluation

Feature selection represents the next critical phase in GEOBIA. Features exerting strong effects on classification accuracy provide a clear distinction between target objects, leading to high within-class similarity and low across-class similarity. Considering the image properties of the study area, five feature categories received full attention after optimal segmentation: spectral features, vegetation index [38, 39], geometric features, position features, and texture features [40]. In total, 90 feature variables were compiled to build the initial feature space **(Table 5)**, along with the formulas for computing each vegetation index **(Table 6)**.

Table 5. Object features.

Feature type	Description
Spectral feature	Includes statistical properties of each spectral band, such as mean band values, standard deviation, brightness, and maximum difference (max_diff).
Vegetation index	Consists of spectral indices and channel combinations, including blue, green, red, EXG, NGBDI, NGRDI, RGRI, and GLI.
Geometry feature	Describes object shape characteristics such as area, length-to-width ratio, length, width, perimeter (border length), shape index, density, compactness, asymmetry, elliptic fit, rectangular fit, and main orientation direction.
Position feature	Captures spatial and temporal location data, including X center, X max, X min, X center (as listed), Y max, Y min, Z center, Z max, Z min, time, time max, time min, and distance to scene boundary.
Texture feature	Includes texture descriptors derived from GLCM and GLDV methods, such as mean, variance, entropy, angular second moment (ASM), homogeneity, contrast, dissimilarity, and correlation, as well as GLDV-based ASM, entropy, mean, and contrast.

Table 6. Vegetation index and calculation formula.

© 2025 The Author(s). | Published by Agro Intelligence Research Press

Vegetation index	Calculation formula
Blue	B/(R + G + B)
Green	G/(R + G + B)
Red	R/(R + G + B)
EXG	2 × G − R − B
NGBDI	(G − B)/(G + B)
NGRDI	(G − R)/(G + R)
RGRI	R/G
GLI	(2 × G − R − B)/(2 × G + R + B)

R, G, and B represent the red, green, and blue bands, respectively.

Optimizing feature selection is essential for high-dimensional datasets to reduce data overlap and improve the model's understanding of key characteristics, thereby strengthening its ability to generalize [41, 42]. The feature space optimization tool in eCognition Developer 9.0 processed all 90 feature variables and provided full details on separability across feature combinations and classes. Using the 1.2 cm spatial-resolution image as an illustration, class separation distances shifted with feature count **(Figure 5)**. At a feature dimension of 45, the separation distance among sample classes reached its highest point (2.949).

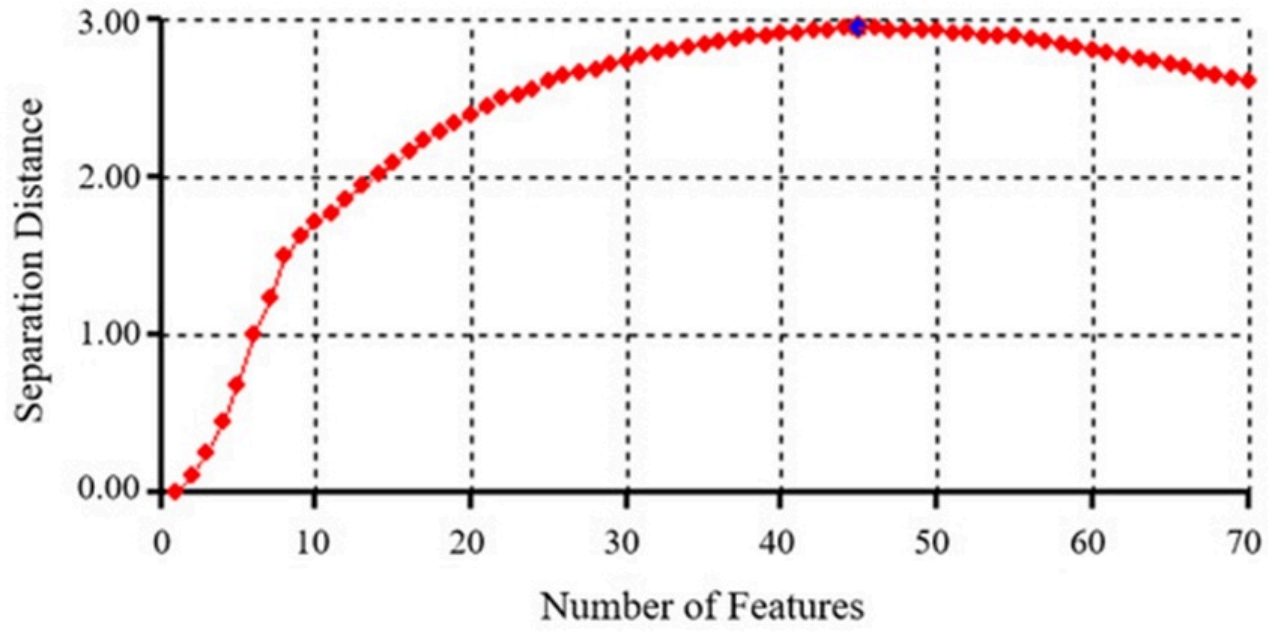

Figure 5. The change in separability between the number of features and classes (1.2 cm spatial resolution image) and the blue diamond (indicating a value of 2.949) was the maximum separation distance.

Even after feature optimization, some variables remained correlated. This study used the mean-decreased-accuracy (MDA) method within RF to further reduce feature dimensions. The approach works by reshuffling original features and measuring how such reordering affects model precision. For less relevant feature variables, reordering causes little change to model accuracy; yet for vital feature variables, reordering lowers model accuracy [43, 44]. Based on the MDA outcomes, all features were ranked by importance from highest to lowest. As a result, 20 to 30 features stayed after

© 2025 The Author(s). | Published by Agro Intelligence Research Press

discarding the least relevant ones. These retained features were used to train RF, SVM, KNN, and Bayes models to detect wetland vegetation species and ground objects in UAV images.

Supervised classification

Machine learning algorithms are non-parametric supervised techniques that have delivered strong results in remote sensing image classification recently [45]. The four classifiers selected here were chosen for their proven value in prior research; however, their success depends heavily on specific parameter choices [46, 47].

RF is an ensemble learning method that assembles numerous trees, with a “decision tree” at its core. A collection of decision trees creates the forest, where each tree produces a classification output, and the class receiving the most votes becomes the final result [48-50]. This research utilized the RF classifier from Python’s Scikit-Learn library. To gauge overall performance, mtry was first set to its default (the square root of the input feature count), and ntree was then increased progressively to 100, 150, 200, and 500. Peak classification performance was observed at ntree = 200. Holding ntree at 200 while shifting mtry away from the default value, either toward smaller or larger values, decreased image classification accuracy. Therefore, when calling the RF classifier in Scikit-Learn, mtry remained at its default value, and ntree was set to 200, conditions that best suited the identification of wetland vegetation species and ground objects in UAV images.

SVM originates from statistical learning theory advanced by Vapnik and colleagues [51]. Its main strength lies in reducing empirical error while simultaneously expanding the classification margin, meaning supervised learning involves locating a hyperplane that maintains classification precision and widens the gap between data categories [52]. SVM includes linear kernel and radial basis function kernels. This study first assessed radial basis function effects on classification and noted inadequate accuracy levels. Consequently, various penalty coefficients C were tested using the linear kernel. Ultimately, setting C to 5 delivered optimal classification performance.

KNN is a widely used nonlinear classifier in which object assignment is based on surrounding samples [53]. If most of the k closest neighboring samples in feature space share the same class, the target sample is assigned to that class [54]. Thus, the k value forms the central parameter for KNN. Values of k from 1 to 10 were tested, with k = 2 yielding the highest classification accuracy.

Bayes functions as a straightforward probabilistic model grounded in Bayes’ theorem, presuming feature independence. The method estimates mean vectors and covariance matrices for each class from training samples before applying them in classification [55]. No parameter adjustments are needed for the Bayes classifier.

Accuracy assessment

This research employed overall accuracy (OA, **Eq. 1**) and the Kappa coefficient to judge the broad classification performance of wetlands on UAV images. OA indicates the probability that classification outputs match the true ground object details. The Kappa coefficient **(Eq. 2)** arises from statistical processing of every entry in the confusion matrix. A multivariate analysis approach was followed, accounting for correctly assigned samples by the model, as well as “commission” and “omission” errors, allowing precise measurement of how well classification outputs correspond to actual ground objects [56].

Producer accuracy (PA, **Eq. 3**), user accuracy (UA, **Eq. 4**), and average PA and UA (AA) were used to measure identification precision for wetland vegetation species and ground objects. PA expresses the share of correctly assigned pixels against the total pixels of that class in the reference data. UA shows the share of correctly assigned pixels against all pixels labeled under that class [57].

In this research, each classifier (RF, SVM, KNN, Bayes) produced 9 Am classification outputs and 8 An classification outputs. These were compared against ground-truth reference images spanning the entire study area, resulting in 68

© 2025 The Author(s). | Published by Agro Intelligence Research Press

accuracy assessments in total.

$$OA = \frac{\sum_{t=1}^{n} X_{tt}}{N} \quad (1)$$

$$Kappa = \frac{N\sum_{t=1}^{n} X_{tt} - \sum_{t=1}^{n} (X_{t+} \times X_{+t})}{N^2 - \sum_{t=1}^{n} (X_{t+} \times X_{+t})} \quad (2)$$

$$PA = \frac{X_{jj}}{X_{+j}} \quad (3)$$

$$UA = \frac{X_{tt}}{X_{t+}} \quad (4)$$

Where N is the total number of evaluation data samples; Xij is the number of samples of class i in the classification result data and class j in the validation data; $\mathrm{X_{i+}} = \sum_{\mathrm{j=1}}^{\mathrm{n}} \mathrm{Xij}$ is the sum of the class i of the classification result; $\mathrm{X_{+j}} = \sum_{\mathrm{i=1}}^{\mathrm{n}} \mathrm{Xij}$ is the sum of class j of the validation data.

Results and Discussion

The optimal SP of the Am and the An

Figure 6 presents the LV and ROC curves for the 1.2 cm resolution image. Clear peaks on the curve appeared at 323, 393, 453, 493, and 543. Using SP values of 453, 493, or 543 produced incomplete divisions for isolated small plants such as lotus and hyacinth. Different plant types were sometimes merged into a single object. Feeding these objects into the RF model gave OA figures of 83.2, 82.4, and 80.1%, with lotus or hyacinth blending into surrounding mixed forest zones. At SP 323, large, uniform categories such as water, construction, and mixed forests showed excessive splitting, resulting in an OA of 81.3%. Outputs were then placed in small vegetation patches, such as mixed grass and hyacinth, within zones designated as pure mixed forest. Setting SP to 393 resulted in proper division of all vegetation types and ground features **(Figure 7)**. This achieved an OA of 85.3% along with minimal errors.

© 2025 The Author(s). | Published by Agro Intelligence Research Press

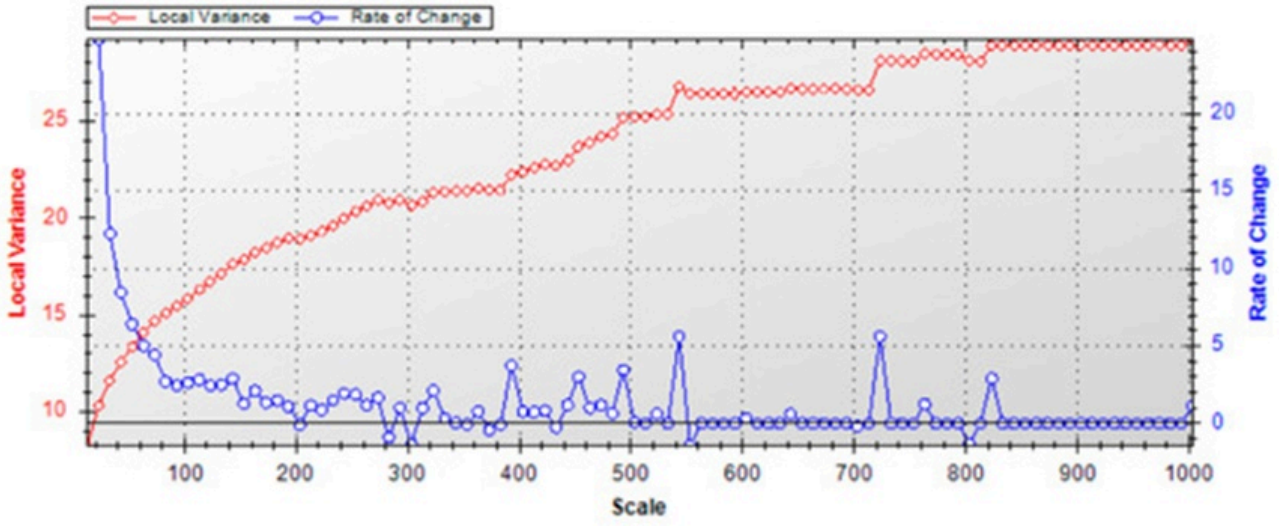

Figure 6. Results of ESP2 scale analysis (1.2 cm spatial resolution image).

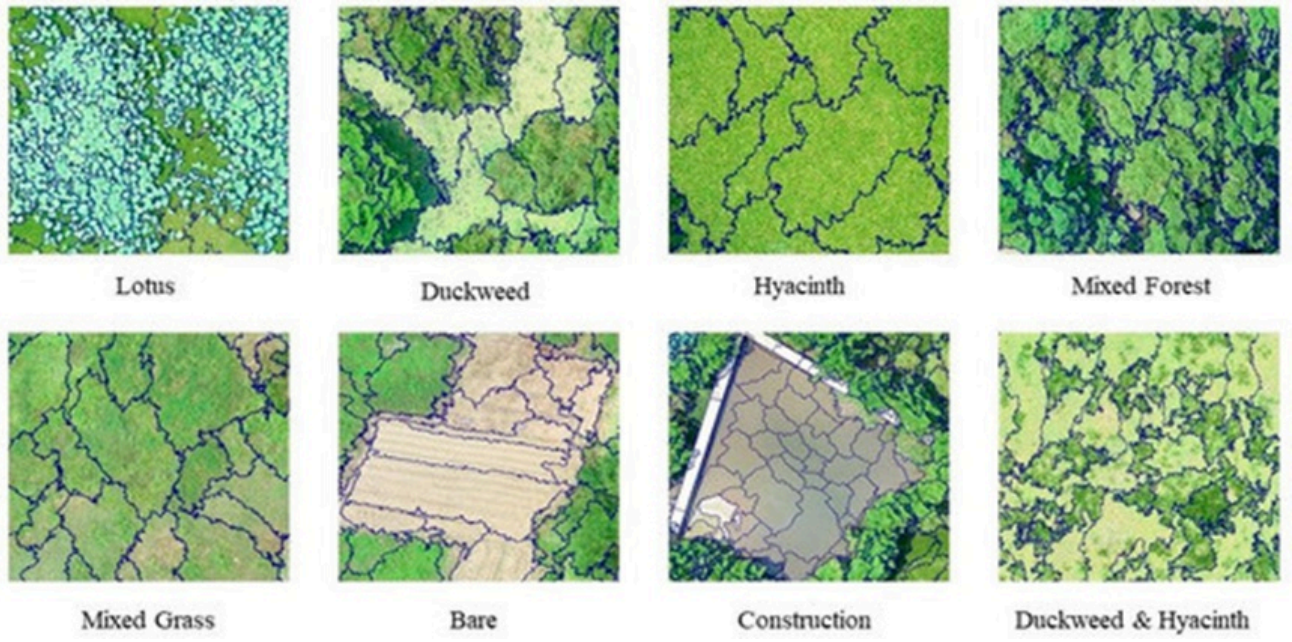

Figure 7. Segmentation results of vegetation species and ground objects (1.2 cm spatial resolution image).

Different spatial scales led to unique optimal SPs **(Figure 8)**. Coarser spatial resolution led to both the best SP and segmentation duration decreasing. Resolutions finer than 1.8 cm demanded SP values above 300 and demanded longer processing. Resolutions from 2.4 to 5.9 cm needed SP settings between 90 and 200, shortening the segmentation period considerably. At matching spatial resolution, SP requirements still differed between Am and An.

© 2025 The Author(s). | Published by Agro Intelligence Research Press

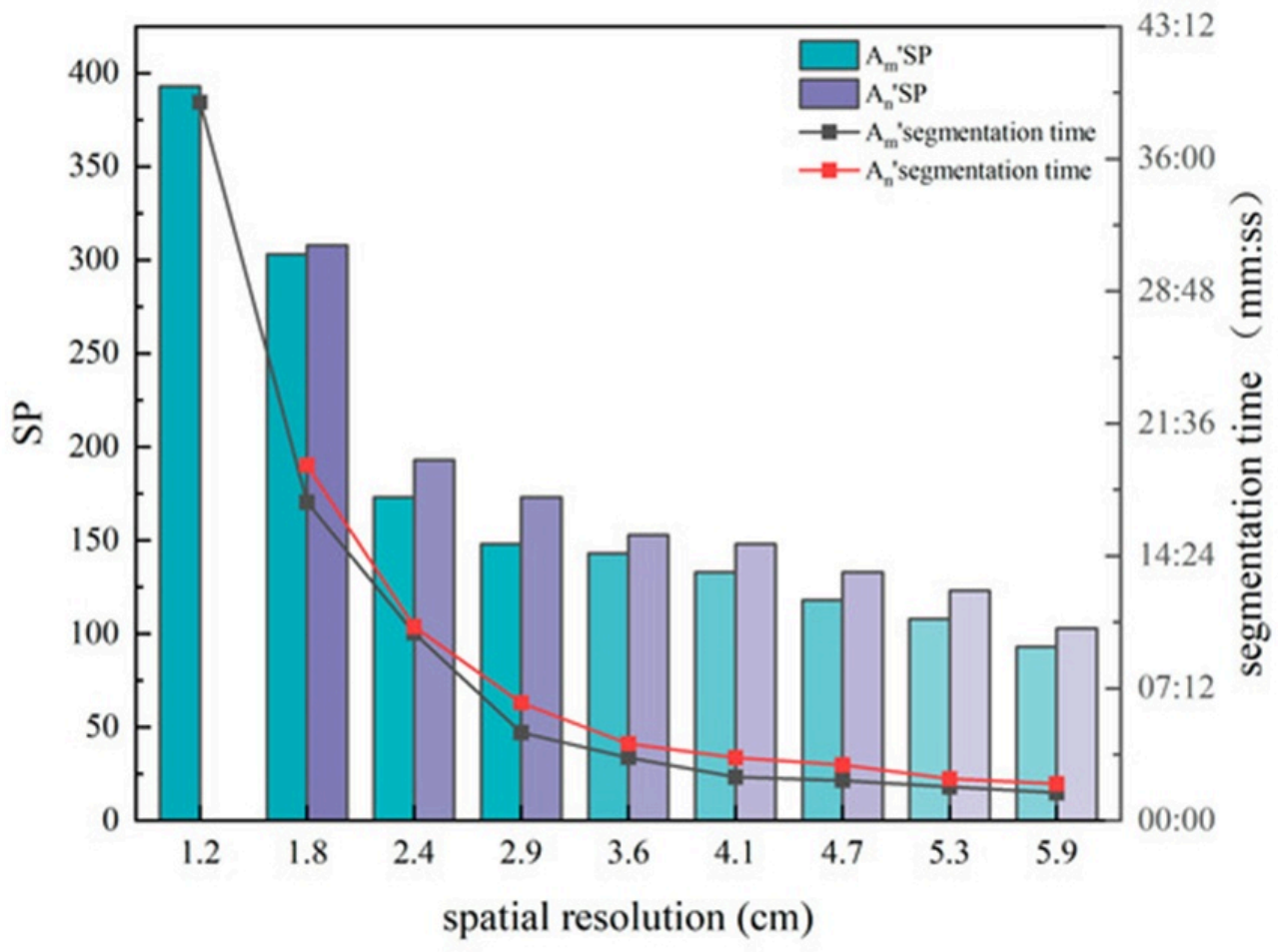

Figure 8. The trend in the optimal SP and segmentation time for Am and An.

Feature selection and evaluation results

The importance of the am feature variables

Feature importance ranking in the Am followed: vegetation index > position features > spectral features > texture features > geometric features **(Figure 9)**. Red, blue, and EXG vegetation indices obtained the strongest scores. Their relative influence shifted with image scale. For ultra-high-resolution identification, X center and Y max emerged as vital position features and performed well across multi-scale assessments. On the 1.2 cm image, X center outweighed the vegetation index and became the leading factor in classification. At 2.9 cm, the Y max led position feature appeared before its role weakened steadily with coarser resolution.

© 2025 The Author(s). | Published by Agro Intelligence Research Press

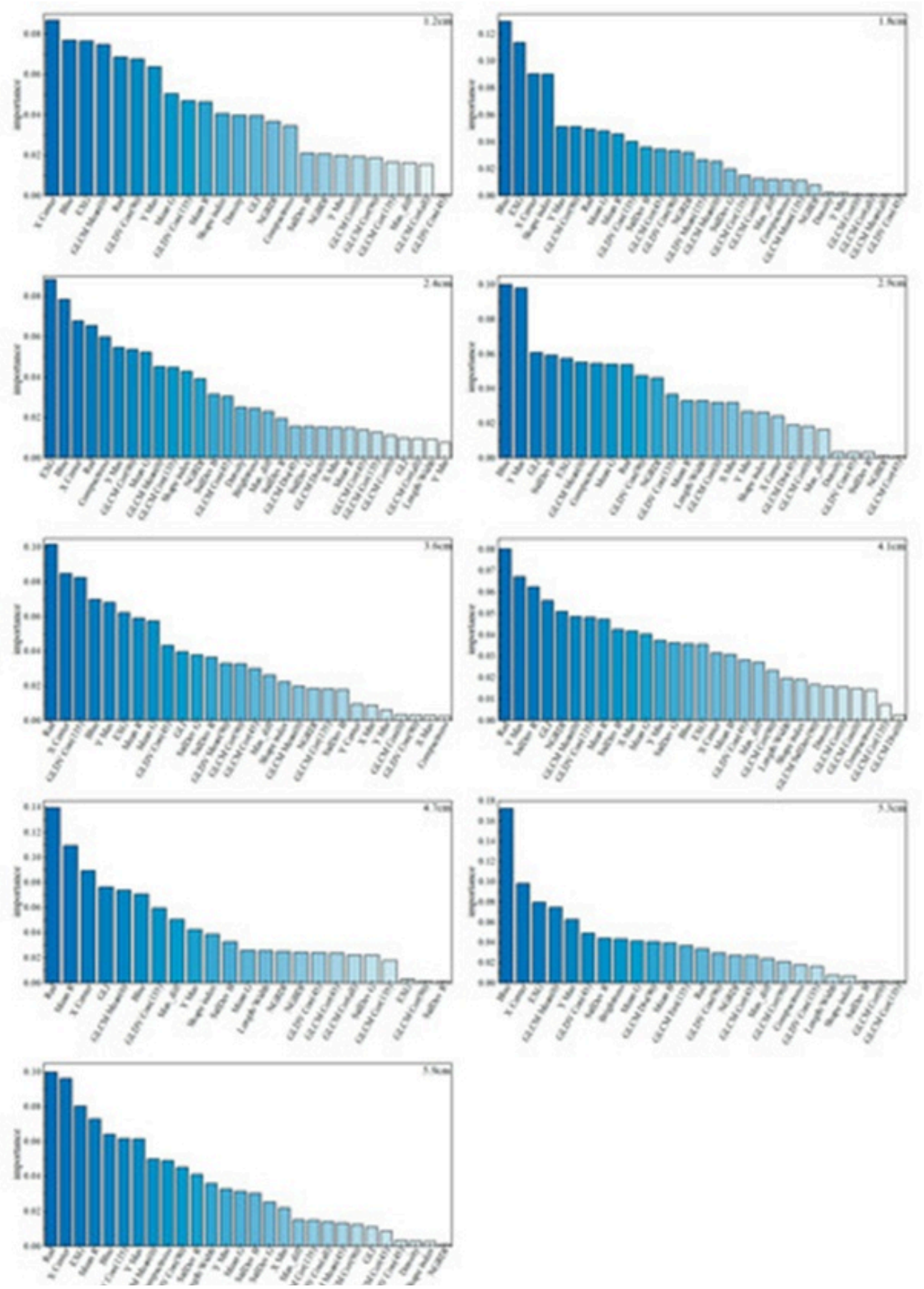

© 2025 The Author(s). | Published by Agro Intelligence Research Press



Spectral and texture features showed varying importance across resolutions. Across scales, mean R, mean G, and stddev B were the primary spectral contributors and exerted a strong influence in the Am. At 2.9 cm, mean R overtook mean G, with the gap widening as resolution fell. Stddev B had the greatest spectral importance at 2.9 cm and affected accuracy most strongly, though its role weakened at both higher and lower resolutions. Stddev R grew steadily more relevant as the resolution coarsened. The GLCM mean (0) remained a core texture element for ultra-high-resolution identification and remained essential in all cases.

Geometric features held lower priority overall. Shape index and compactness showed weak effects from 1.8 to 2.9 cm, with shape index strongest at 1.8 cm. Its importance faded as the resolution moved away in either direction.

The importance of the An feature variables

Feature importance order in the An was: vegetation index > position features > spectral features > texture features > geometric features **(Figure 10)**, closely matching the Am pattern. Blue and EXG stood out most strongly across scales and drove identification accuracy for wetland plants and surface features. Red held notable weight from 1.8 to 3.6 cm but dropped sharply from 4.1 to 5.9 cm. X center led position features, with Y max next. Other position variables added almost no value to accuracy.

© 2025 The Author(s). | Published by Agro Intelligence Research Press

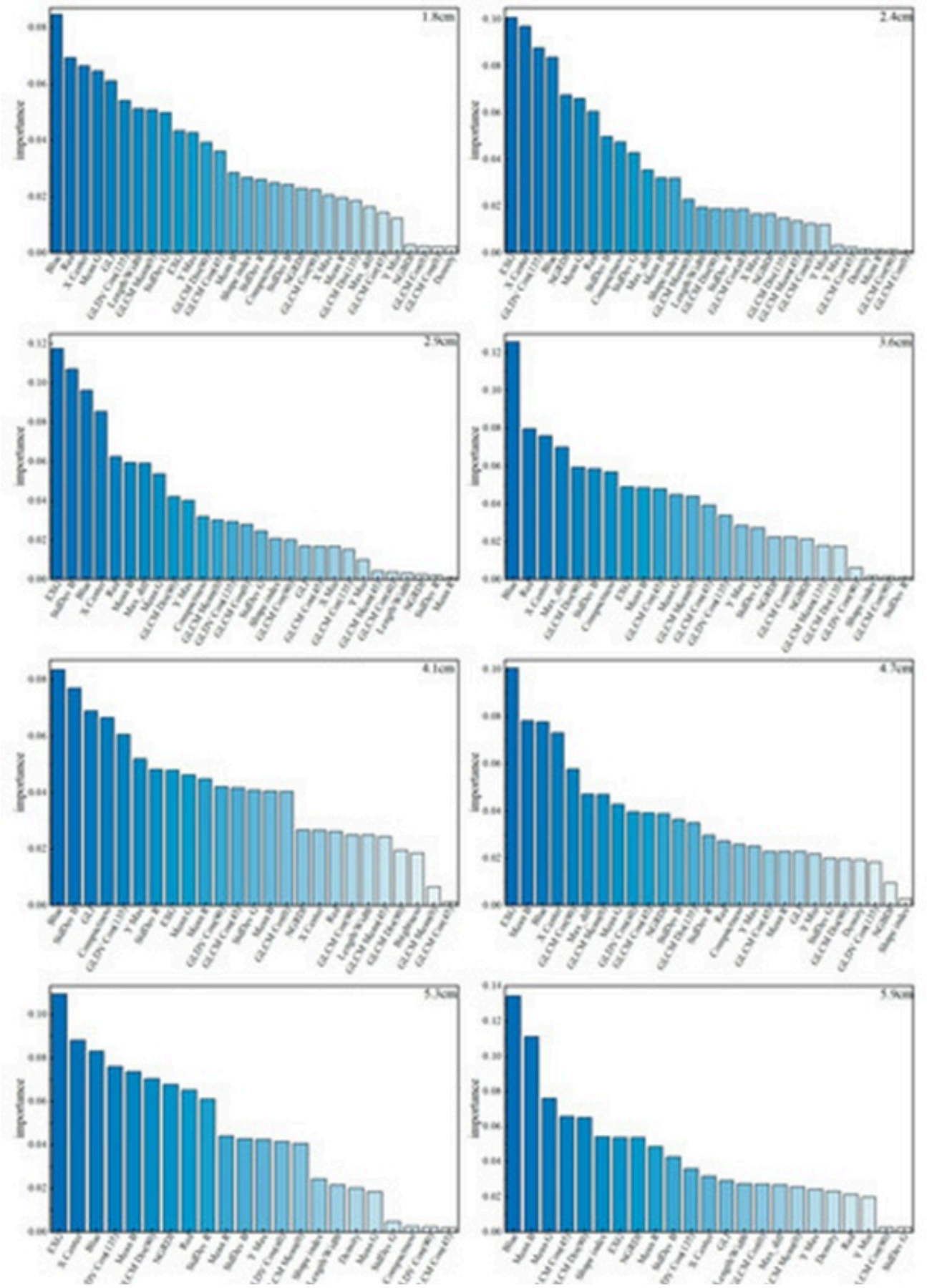

© 2025 The Author(s). | Published by Agro Intelligence Research Press



Mean G, mean B, and stddev B showed strong spectral importance. Stddev B rose in relevance with coarser resolution, peaked at 2.9 cm, then fluctuated mildly downward. Mean B mattered little from 1.8 to 4.1 cm, yet became highly influential from 4.7 to 5.9 cm. Max_diff gained steadily from 1.8 to 3.6 cm and topped spectral features at 3.6 cm. Leading texture contributors in the An included GLDV contrast (135), GLCM dissimilarity (90), and GLCM mean (0). GLCM correlation (90) was significant only at 4.7 cm and remained minor elsewhere.

Geometric features carried limited weight in the An. Compactness led from 2.4 to 4.7 cm. The shape index overtook compactness and became dominant at 5.3-5.9 cm.

Overall classification accuracy

Overall classification accuracy of the Am

OA and Kappa values in the Am first climbed, then dropped with decreasing spatial resolution, reaching their highest at 2.9 cm **(Table 7)**. All classifiers displayed matching change patterns for Am results. From 1.2 to 2.9 cm, RF, SVM, and KNN produced similar OA levels (85.2%–88.8%) that beat Bayes. From 3.6 to 5.9 cm, SVM outperformed RF, with the difference expanding at coarser resolutions. Below 2.9 cm, KNN performance plunged and trailed Bayes at 5.3 cm.

Table 7. Overall classification accuracy of each classifier in the Am.

	Resolution (cm)	5.9	5.3	4.7	4.1	3.6	2.9	2.4	1.8	1.2
Classifier										**s**
RF	OA	82.1%	83.9%	84.4%	85.1%	85.9%	88.8%	87.3%	85.9%	85.3%
	Kappa	0.768	0.790	0.797	0.807	0.817	0.855	0.835	0.816	0.808
SVM	OA	84.2%	84.5%	85.1%	85.1%	86.2%	88.3%	86.8%	85.7%	85.2%
	Kappa	0.797	0.800	0.807	0.808	0.822	0.849	0.831	0.815	0.809
KNN	OA	77.3%	78.6%	80.7%	82.4%	83.4%	88.3%	87.2%	86.0%	85.5%
	Kappa	0.714	0.730	0.749	0.775	0.787	0.850	0.836	0.820	0.814
Bayes	OA	79.5%	79.8%	80.2%	81.3%	82.1%	85.0%	83.9%	82.1%	81.3%
	Kappa	0.736	0.735	0.744	0.759	0.767	0.807	0.792	0.769	0.768

Overall classification accuracy of the An

OA and Kappa patterns for the four classifiers in the An largely mirrored the Am, peaking at 2.9 cm **(Table 8)**. RF delivered the strongest results overall. KNN surpassed SVM from 1.2 to 2.4 cm. From 2.9 to 5.9 cm, SVM took the lead over KNN, with steadier shifts.

Table 8. Overall classification accuracy of each classifier in the An.

	Resolution (cm)	1.2	5.9	5.3	4.7	4.1	3.6	2.9	2.4	1.8
Classifier										
RF	OA	/	88.4%	88.5%	88.6%	88.8%	89.3%	91.2%	89.1%	87.0%
	Kappa	/	0.850	0.850	0.852	0.850	0.861	0.886	0.860	0.832

© 2025 The Author(s). | Published by Agro Intelligence Research Press

SVM	OA	/	88.1%	88.1%	88.2%	88.2%	88.9%	91.2%	88.0%	86.6%
	Kappa	/	0.846	0.846	0.848	0.848	0.857	0.887	0.846	0.827
KNN	OA	/	87.8%	87.9%	87.9%	88.2%	88.2%	90.8%	88.7%	86.7%
	Kappa	/	0.842	0.842	0.842	0.846	0.847	0.883	0.855	0.831
Bayes	OA	/	84.0%	85.5%	85.7%	85.9%	86.4%	86.8%	85.2%	82.0%
	Kappa	/	0.796	0.811	0.816	0.816	0.824	0.830	0.810	0.767

Identification accuracy of vegetation species and ground objects

Owing to RF's better performance than SVM, KNN, and Bayes, classification outputs for vegetation species and ground objects came from the RF classifier. PA, UA, and AA measured identification precision.

Identification accuracy of vegetation species and ground objects in the Am

Major mismatches between Am outputs and the ground-truth reference occurred in the northern, northeastern, and southern zones, as shown in red in **Figure 11**. Across scales, northern hyacinth, duckweed, and lotus faced frequent commission or omission. From 4.7 to 5.9 cm, northeastern mixed grass was often misidentified as hyacinth. At 1.2, 1.8, and 3.6–5.9 cm, southern mixed grass areas were mislabeled as mixed forest. Water and construction matched reference data well. PA, UA, and AA revealed the spatial scale influence of the Am.

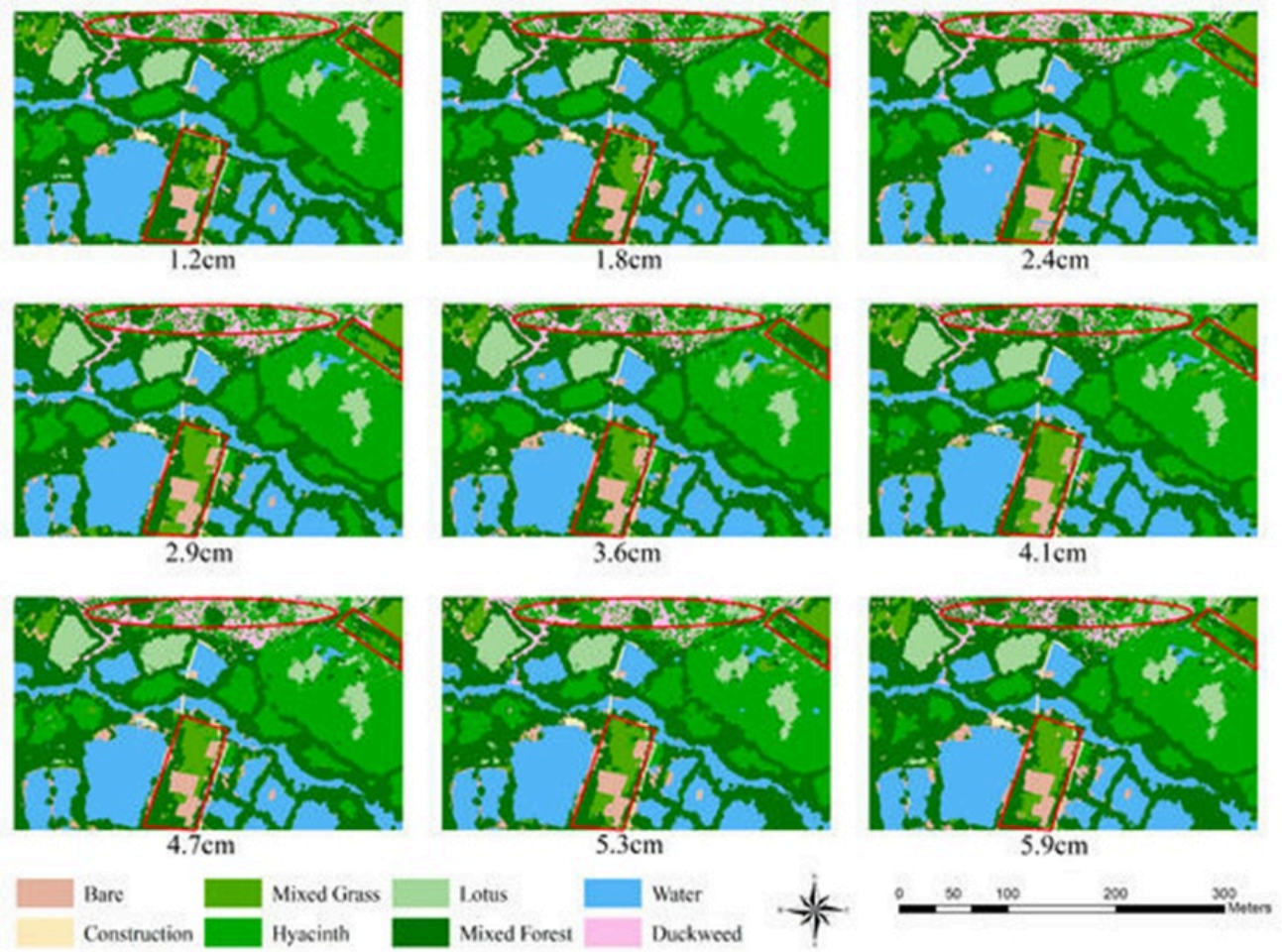

© 2025 The Author(s). | Published by Agro Intelligence Research Press

Figure 11. The Am classification results from the RF classifier; the UAV-RGB image and ground-truth reference image of the study area are shown in **Figures 1 and 2**, respectively.

Resolution shifts had a barely detectable effect on water detection in the Am. Water achieved the top PA, UA, and AA (near 95%) at all scales. Hyacinth, mixed forest, and construction had close PA values (86, 91, 90%) at 1.2-2.9 cm, which then declined with coarser resolution. Lotus and bare followed similar PA trends, rising then falling, with peaks of 88.1% and 82.6% at 1.8 cm. Mixed grass and duckweed PA fluctuated widely. Duckweed peaked at 2.4 and 2.9 cm. UA for lotus, hyacinth, mixed forest, and construction stayed comparable and fell steadily with coarser resolution. Duckweed had the weakest UA across all scales. Lotus, hyacinth, and barley reached their highest AA at 1.8 cm; mixed forest, mixed grass, and duckweed peaked at 2.4 and 2.9 cm **(Figure 12)**.

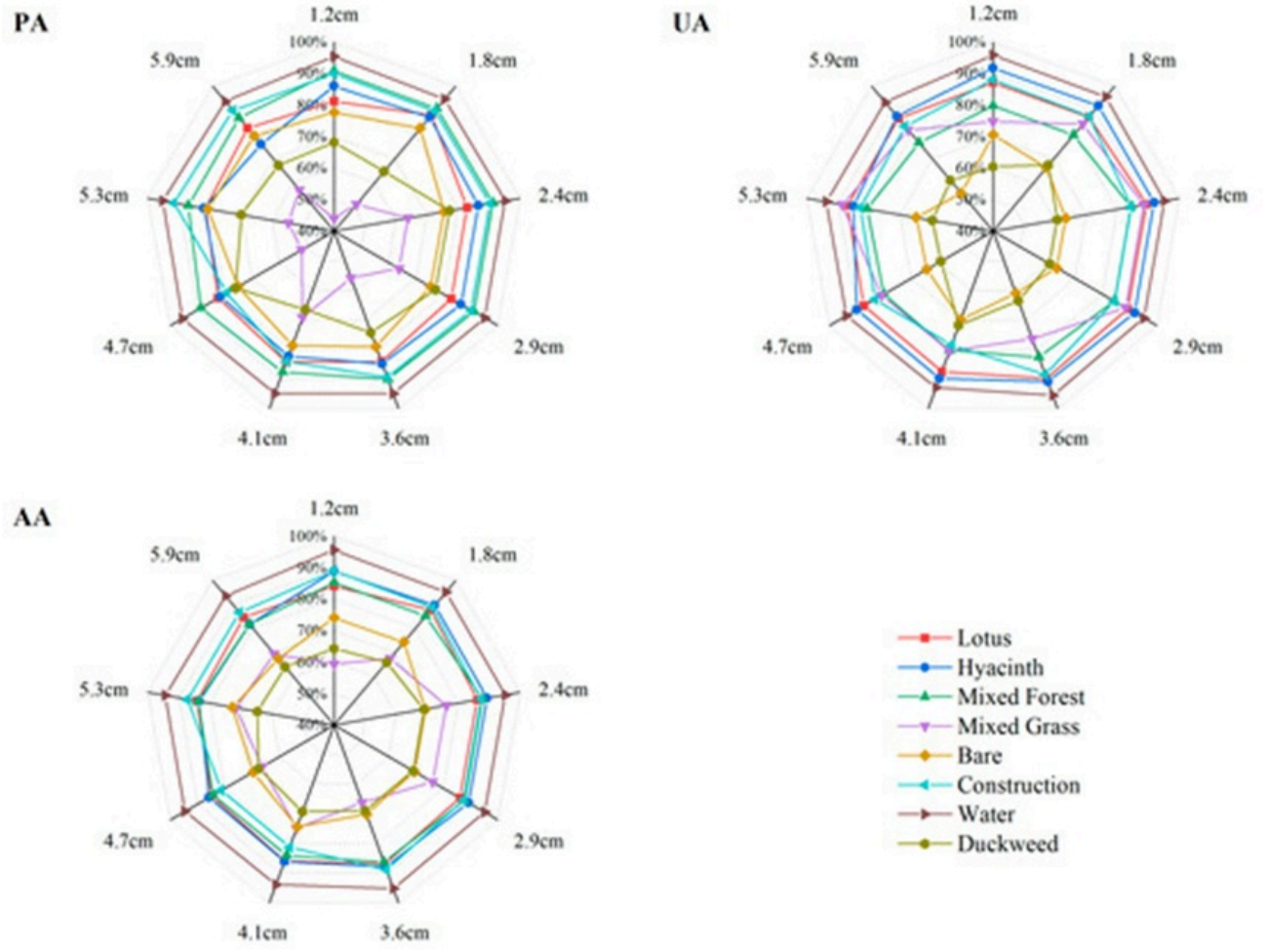

Figure 12. Identification accuracy of vegetation species and ground objects in the Am.

Identification accuracy of vegetation species and ground objects in the An

The most noticeable mismatches between the An classification outputs and ground-truth reference images occurred in the northern and northeastern sections of the study area, highlighted in red in **Figure 13**. Hyacinth, duckweed, lotus, and mixed forests in the northern section of the An outputs showed a greater tendency toward commission or omission errors. Mixed grass in the northeastern section was also frequently mislabeled as mixed forest. Consistent with Am outputs, the water and construction classifications in the An aligned reasonably well with the ground-truth reference images.

© 2025 The Author(s). | Published by Agro Intelligence Research Press

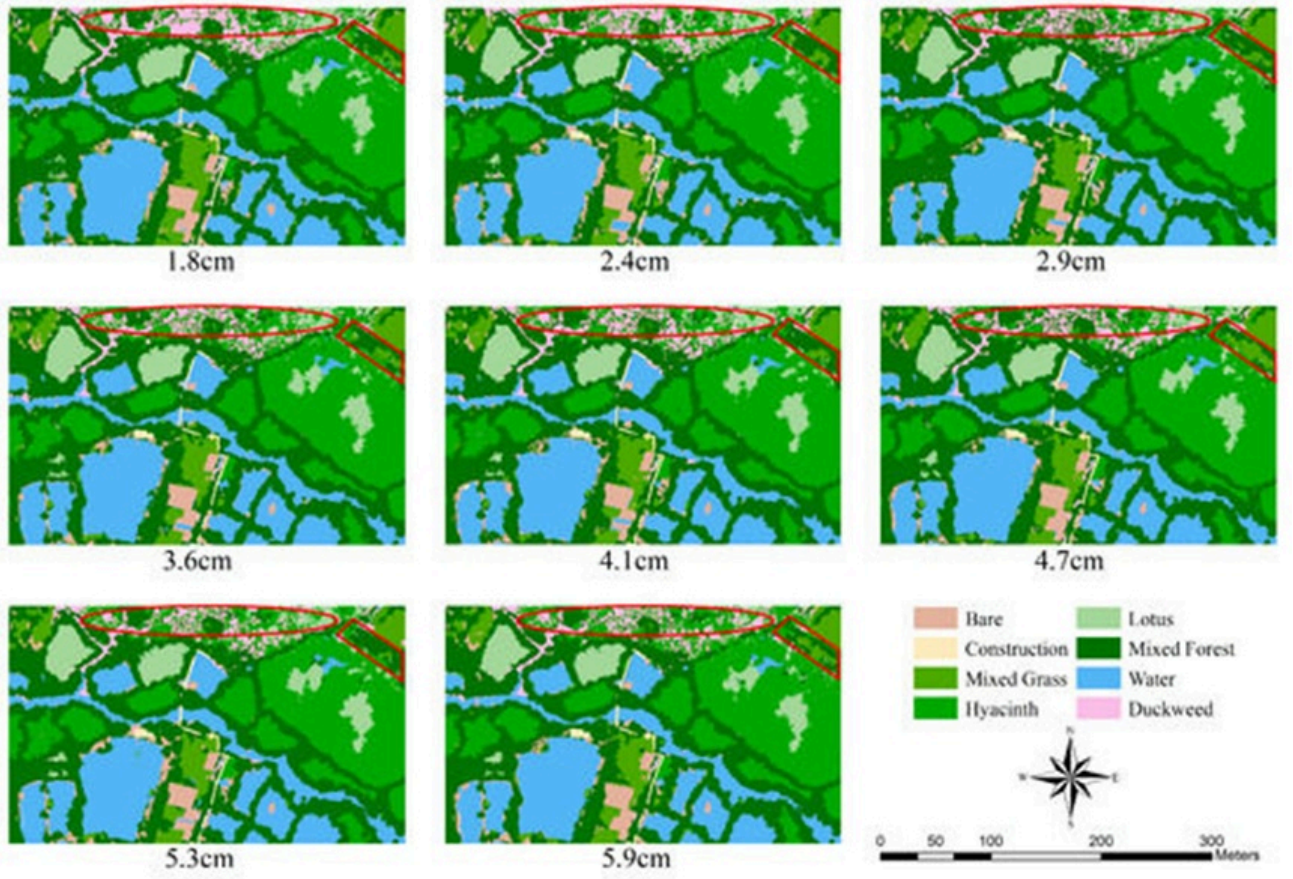

Figure 13. The An classification results under the RF classifier; the UAV-RGB image and ground truth reference image in the study area are shown in **Figures 1 and 2**, respectively.

In the An outputs, water maintained the strongest PA, UA, and AA values throughout the multi-scale images **(Figure 14)**. Spatial resolution clearly influenced PA for lotus, mixed forest, bare, and duckweed, with these metrics rising first and then falling as resolution decreased, reaching a peak at 2.9 cm. Mixed grass recorded the lowest PA relative to other categories in multi-scale images. Lotus, hyacinth, and mixed grass showed comparable spatial-scale patterns in UA as well. UA values initially increased before declining with coarser resolution, reaching a maximum of 2.9 cm. Overall, hyacinth achieved the best UA, followed by lotus and then mixed grass. AA values for lotus, hyacinth, duckweed, mixed forest, bare, construction, and water showed a similar response pattern to changes in spatial resolution. AA rose from 1.8 to 2.9 cm and then declined from 2.9 to 5.9 cm.

© 2025 The Author(s). | Published by Agro Intelligence Research Press

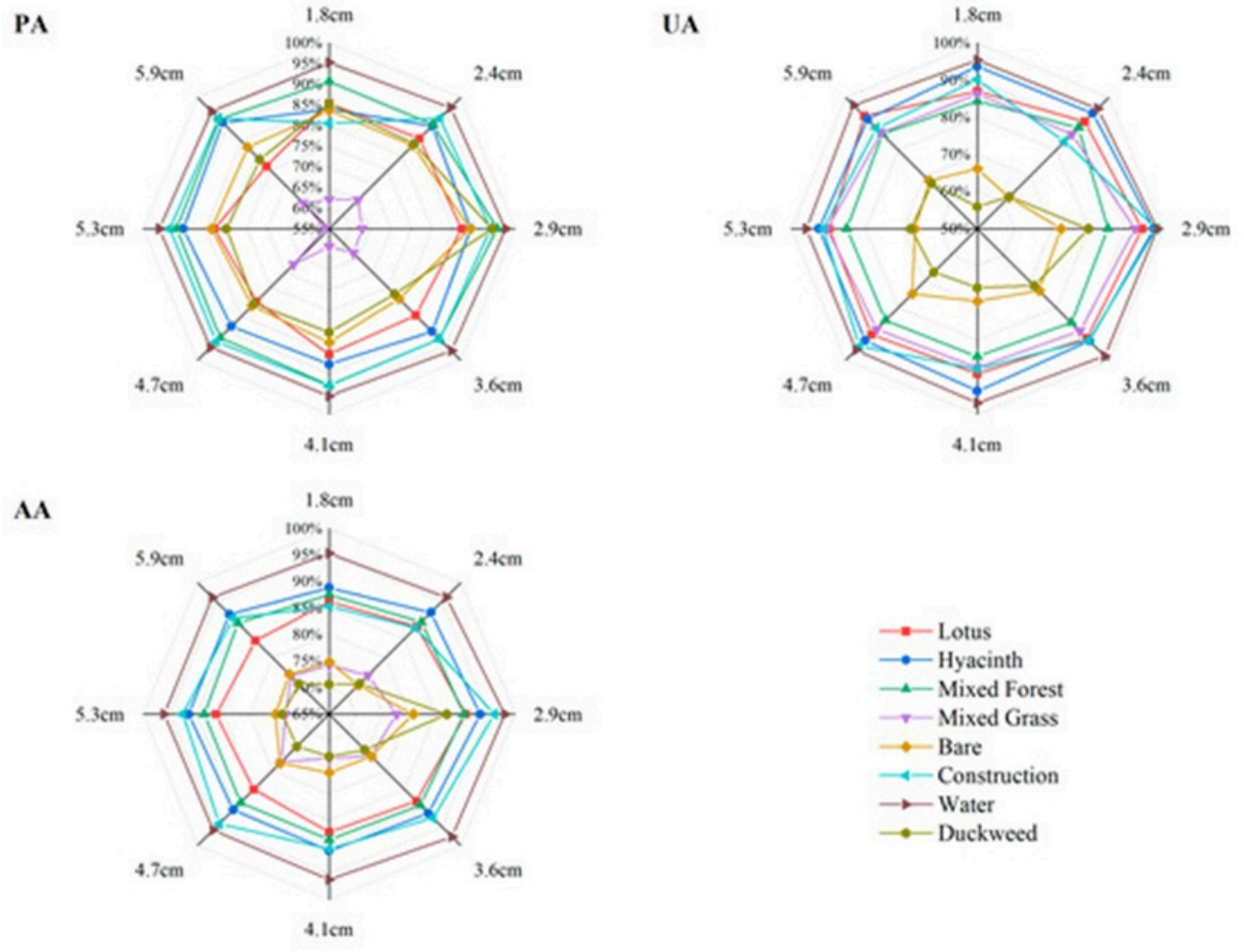

Figure 14. Identification accuracy of vegetation species and ground objects in the An results.

As a widely adopted method for remote sensing image classification, GEOBIA has been extensively applied to map wetland vegetation species and ground objects [58]. Within this framework, image segmentation is the primary and most critical stage. Earlier studies have shown that the FNEA multi-resolution segmentation algorithm is among the most widely used approaches for identifying wetland vegetation and other surface objects. The choice of segmentation parameters strongly determines the size of the resulting image objects and directly affects the accuracy of vegetation and ground object extraction. For this reason, identifying an optimal parameter set is essential for reliable wetland classification [32].

The FNEA multi-resolution approach relies on three main parameters: shape, compactness, and SP. Among these, SP variations influence segmentation quality more strongly than adjustments in shape and compactness [59]. In this study, shape and compactness were set to 0.2 and 0.5 through iterative testing, while SP was determined using the ESP2 tool to minimize subjective bias. However, most previous research on optimal SP values has been limited to images with a single spatial resolution, leaving open the question of how aerial and resampled datasets with different resolutions behave.

The results showed that higher spatial resolution led to longer processing times and larger optimal SP values **(Figure 8)**. This occurs because higher-resolution imagery produces larger datasets, thereby increasing computational load. Therefore, future work should place greater emphasis on processing efficiency rather than focusing only on maximizing spatial resolution during UAV data collection. Even when spatial resolution remained constant, the optimal SP for the An was slightly higher than for the Am. This is likely because resampling reduced internal variability in the An image, allowing

© 2025 The Author(s). | Published by Agro Intelligence Research Press

a higher SP to still produce segmentation comparable to the Am. Using the optimized parameters, vegetation types and ground objects were successfully separated, with object boundaries closely matching real-world features, making them suitable for further analysis.

In GEOBIA, feature selection is the second key stage after segmentation. Because UAV-RGB images have limited spectral information and strong spectral overlap among wetland vegetation types, this study integrated vegetation indices, texture metrics, positional variables, and geometric descriptors to compensate for spectral limitations. However, using too many variables can introduce redundancy and lead to overfitting, thereby reducing classification performance. To address this, a feature space optimization tool, combined with the MDA method, was used to improve handling of high-dimensional data and to evaluate feature importance.

Consistent with previous research, vegetation indices generally ranked highest in importance, while geometric features ranked lowest in importance [41, 60]. Interestingly, this study found that positional variables contributed more than expected, especially X center and Y max. This may be due to the spatially restricted nature of the study area, where location-based features became more informative. As a result, these positional features can improve classification performance in small-scale wetland mapping tasks. In contrast, geometric variables showed consistently low importance, suggesting they should be used cautiously in future work.

When comparing Am and An, key vegetation indices and texture features, such as red, blue, EXG, and GLCM mean (0), were among the most influential variables, indicating their importance in classification tasks. Noticeable differences were also observed between datasets. For example, max_diff in the An showed stronger spectral importance than in the Am. In terms of texture, GLDV contrast (135), GLCM dissimilarity (90), and GLCM correlation (90) were more influential in the An, which may help explain why the An achieved higher classification accuracy than the Am in the final results.

RF, SVM, KNN, and Bayes are commonly applied machine learning algorithms for image classification. In this study, their ability to classify wetland vegetation species and ground objects was evaluated using OA and kappa statistics. In line with earlier studies, performance differs among classifiers, with RF typically delivering the strongest results [55]. For this reason, RF should be prioritized in future wetland classification work. This research mainly investigated how these four classifiers respond to varying spatial resolutions, and the results showed that OA and kappa patterns were generally consistent across both the Am and An models. When the spatial resolution fell below 2.9 cm, both OA and kappa values dropped sharply **(Tables 7 and 8)**, mainly due to an increase in mixed pixels resulting from lower resolution. In such pixels, multiple land-cover types coexist, and the final label depends on their relative proportions. This leads to small or fragmented classes being absorbed by larger, more uniform ones, while boundary regions are especially prone to omission and commission errors [61].

Nevertheless, increasing spatial resolution does not always improve outcomes [24]. For example, imagery at 1.2, 1.8, and 2.4 cm produced lower accuracy than imagery at 2.9 cm. This is because vegetation and ground objects have inherent physical scales, and exceeding an optimal resolution can actually reduce separability [62, 63]. While ultra-high-resolution images provide fine spatial detail, they also amplify within-class variability, making identical vegetation types appear more heterogeneous and harder to distinguish. At the same time, they introduce substantial redundancy in information, which reduces computational efficiency [62, 64]. As a result, future work should avoid focusing solely on achieving the highest possible resolution, and UAV flight altitude should be optimized to balance coverage and efficiency while maintaining accuracy. The results further showed that the An consistently outperformed the Am, likely because pixel-aggregation resampling reduced internal spectral and textural variability while increasing separability between different classes compared with raw aerial imagery [20, 65]. Thus, resampled data appear more effective than aerial data for wetland classification within the 1.2–5.9 cm resolution range.

Using the RF model, this study also examined how spatial scale influences the classification performance of different vegetation and ground object types, guiding the selection of suitable image resolution for wetland mapping. UA, PA, and AA were calculated for each class in both Am and An **(Figures 12 and 14)**. Results indicated that water maintained

© 2025 The Author(s). | Published by Agro Intelligence Research Press

consistently high accuracy across both datasets, likely because it forms relatively homogeneous segments after FNEA segmentation. In addition, water is visually and spectrally distinct from other categories, making it easier to extract in wetland environments.

Figure 12 further showed that in the Am, finer resolutions (1.2–2.9 cm) were required to improve PA for hyacinth, mixed forest, and construction. Meanwhile, duckweed exhibited the lowest UA in the Am, mainly because it was concentrated in the northern part of the study area, where vegetation was highly fragmented. It is also frequently mixed with hyacinth, and its irregular shape across scales made it difficult to classify accurately.

In the An, mixed grass had the lowest PA, while mixed forest achieved higher PA. This is likely because mixed grass often occurs along the edges of mixed forest and is therefore easily confused with it, leading to misclassification. The optimal resolution also varied across datasets. In the Am, classes such as lotus, hyacinth, and bare land reached their best AA at 1.8 cm, while mixed forest, mixed grass, and duckweed performed best at 2.4 or 2.9 cm.

By contrast, the An showed more stable resolution-dependent behavior because it was derived from a single dataset using pixel aggregation, which ensured more consistent image characteristics across scales. The Am, acquired at different UAV flight heights, was more affected by environmental conditions, such as wind and illumination, leading to greater variability. In the An, extremely fine resolutions (1.8–2.4 cm) introduced noise, while coarser ones (3.6–5.9 cm) caused excessive pixel mixing, limiting separability. The 2.9 cm resolution, therefore, represented a balance between detail and noise reduction, making it the most suitable for wetland classification.

Conclusion

This study involved flying UAVs at several altitudes across the study area to capture aerial images (Am) at varying spatial resolutions. The 1.2 cm spatial-resolution aerial image was then resampled to create resampled images (An) that matched the spatial resolution of the Am. Applying the GEOBIA method, multiple machine learning classifiers were used to classify vegetation species and ground objects for both the Am and the An, leveraging optimal segmentation results and feature selection. The study produced these conclusions:

(1) During the image segmentation phase of GEOBIA, SP is the most vital parameter in the multi-resolution segmentation algorithm. Selecting proper SP values for images at different spatial resolutions proves necessary to achieve clear separation of all vegetation species and ground objects. In this study, the optimal SP applied to the resampled image exceeded the value used for the aerial image at identical spatial resolution. Optimal SP values decreased steadily as spatial resolution decreased, resulting in a substantial drop in required segmentation time.

(2) In the feature selection phase of GEOBIA, varying feature variables become necessary for images possessing different spatial resolutions. Aerial images and resampled images exhibit differences in spectral or texture information arising from their distinct imaging mechanisms. For instance, this study found that importance levels for certain spectral features and texture features were higher in the An than in the Am. Feature variable importance ranking for both the Am and the An followed this order: vegetation index > position feature > spectral feature > texture feature > geometric feature. Hence, future studies must choose suitable feature variables tailored to images with specific spatial resolutions and imaging mechanisms to safeguard classification accuracy.

(3) Across the spatial resolution range of 1.2 to 5.9 cm, resampled images usually delivered stronger classification accuracy than aerial images. In addition, the RF classifier achieved greater overall classification accuracy and outperformed SVM, KNN, and Bayes classifiers. Once spatial resolution fell below a particular threshold, small and fragmented classes faced a higher risk of misclassification due to the mixed-pixel effect. The ideal resolution emerged when the spectrum or texture showed minimal variation within classes and maximal variation between classes.

© 2025 The Author(s). | Published by Agro Intelligence Research Press

(4) The same vegetation species or ground object produced differing PA, UA, and AA values when classified using images at varying spatial resolutions. Achieving elevated classification accuracy in UAV flight experiments and subsequent data processing requires careful selection of spatial resolution images according to the distribution patterns and patch dimensions of each vegetation species and ground object inside the target study area. Importantly, optimal spatial resolution for identical vegetation species or ground objects varied between aerial images and resampled images. For example, in this study, the Am yielded the highest extraction accuracy for lotus and hyacinth at 1.8 cm and for duckweed at 2.4 and 2.9 cm. In contrast, the An found the 2.9 cm image most effective for identifying lotus, hyacinth, and duckweed.

Acknowledgements

None

Conflict of interest

None

Financial support

This study was supported by grants from Guangxi Science and Technology Base and Talent Project (GuikeAD19245032), Major Special Projects of High Resolution Earth Observation System (84-Y50G25-9001-22/23), the National Natural Science Foundation of China (41801030, 41861016), Guangxi Key Laboratory of Spatial Information and Geomatics (19-050-11-22), and Research Foundation of Guilin University of Technology (GUTQDJJ2017069).

Ethics statement

None

Received: 08 Oct 2023 Revised: 13 Dec 2023 Accepted: 29 Dec 2023
Published online: 25 May 2025

Rights and permissions

Open Access The author(s) retain copyright. This article is licensed under the Creative Commons Attribution-NonCommercial-ShareAlike 4.0 International License. It may be shared and adapted for non-commercial purposes with appropriate attribution, an indication of changes, and distribution of adaptations under the same license. Third-party material may be subject to separate terms identified in its credit line. View the license at https://creativecommons.org/licenses/by-nc-sa/4.0/.

References

1. Wang Z, Wu J, Madden M, Mao D. China's wetlands: Conservation plans and policy impacts. Ambio. 2012;41:782–86.

2. Yang Y, Chen J, Lan Y, Zhou G, You H, Han X, et al. Landscape pattern and ecological risk assessment in Guangxi based on land use change. Int J Environ Res Public Health. 2022;19:1595.

3. Davidson NC. How much wetland has the world lost? Long-term and recent trends in global wetland area. Mar Freshw Res. 2014;65:934–41.

4. Koch M, Schmid T, Reyes M, Gumuzzio J. Evaluating full polarimetric C- and L-band data for mapping wetland conditions in a semi-arid environment in central Spain. IEEE J Sel Top Appl Earth Obs Remote Sens. 2012;5:1033–44.

5. Fu B, Zuo P, Liu M, Lan G, He H. Classifying vegetation communities karst wetland synergistic use of image fusion and object-based machine learning algorithm with Jilin-1 and UAV multispectral images. Ecol Indic. 2022;140:108989.

6. Davidson NC, Fluet-Chouinard E, Finlayson CM. Global extent and distribution of wetlands: Trends and issues. Mar Freshw Res. 2018;69:620–7.

7. Dronova I. Object-based image analysis in wetland research: A review. Remote Sens. 2015;7:6380–413.

8. Adam E, Mutanga O, Rugege D. Multispectral and hyperspectral remote sensing for identification and mapping of wetland vegetation: A review. Wetl Ecol Manag. 2009;18:281–96.

9. Guo M, Li J, Sheng C, Xu J, Wu L. A review of wetland remote sensing. Sensors. 2017;17:777.

10. Tana G, Letu H, Cheng Z, Tateishi R. Wetlands mapping in North America by decision rule classification using MODIS and ancillary data. IEEE J Sel Top Appl Earth Obs Remote Sens. 2013;6:2391–401.

11. McCarthy MJ, Merton EJ, Muller-Karger FE. Improved coastal wetland mapping using very-high 2-meter spatial resolution imagery. Int J Appl Earth Obs Geoinf. 2015;40:11–8.

12. Chen Y, He X, Xu J, Zhang R, Lu Y. Scattering feature set optimization and polarimetric SAR classification using object-oriented RF-SFS algorithm in coastal wetlands. Remote Sens. 2020;12:407.

13. Chen J, Zhao X, Zhang H, Qin Y, Yi S. Evaluation of the accuracy of the field quadrat survey of alpine grassland fractional vegetation cover based on the satellite remote sensing pixel scale. ISPRS Int J Geo-Inf. 2019;8:497.

14. Chen J, Yi S, Qin Y, Wang X. Improving estimates of fractional vegetation cover based on UAV in alpine grassland on the Qinghai-Tibetan Plateau. Int J Remote Sens. 2016;37:1922–36.

15. Chen J, Huang R, Yang Y, Feng Z, You H, Han X, et al. Multi-scale validation and uncertainty analysis of GEOV3 and MuSyQ FVC products: A case study of an alpine grassland ecosystem. Remote Sens. 2022;14:5800.

16. Arif MSM, Gülch E, Tuhtan JA, Thumser P, Haas C. An investigation of image processing techniques for substrate classification based on dominant grain size using RGB images from UAV. Int J Remote Sens. 2016;38:2639–61.

17. Rominger K, Meyer S. Application of UAV-based methodology for census of an endangered plant species in a fragile habitat. Remote Sens. 2019;11:719.

18. Sankey JB, Sankey TT, Li J, Ravi S, Wang G, Caster J, et al. Quantifying plant-soil-nutrient dynamics in rangelands: Fusion of UAV hyperspectral-LiDAR, UAV multispectral-photogrammetry, and ground-based LiDAR-digital photography in a shrub-encroached desert grassland. Remote Sens Environ. 2021;253:112223.

19. Yan G, Li L, Coy A, Mu X, Chen S, Xie D, et al. Improving the estimation of fractional vegetation cover from UAV RGB imagery by colour unmixing. ISPRS J Photogramm Remote Sens. 2019;158:23–34.

20. Roth KL, Roberts DA, Dennison PE, Peterson SH, Alonzo M. The impact of spatial resolution on the classification of plant species and functional types within imaging spectrometer data. Remote Sens Environ. 2015;171:45–57.

© 2025 The Author(s). | Published by Agro Intelligence Research Press

21. Meddens AJH, Hicke JA, Vierling LA. Evaluating the potential of multispectral imagery to map multiple stages of tree mortality. Remote Sens Environ. 2011;115:1632–42.

22. Hu P, Guo W, Chapman SC, Guo Y, Zheng B. Pixel size of aerial imagery constrains the applications of unmanned aerial vehicle in crop breeding. ISPRS J Photogramm Remote Sens. 2019;154:1–9.

23. Liu M, Yu T, Gu X, Sun Z, Yang J, Zhang Z, et al. The impact of spatial resolution on the classification of vegetation types in highly fragmented planting areas based on unmanned aerial vehicle hyperspectral images. Remote Sens. 2020;12:146.

24. Lu B, He Y. Optimal spatial resolution of unmanned aerial vehicle (UAV)-acquired imagery for species classification in a heterogeneous grassland ecosystem. GIScience Remote Sens. 2017;55:205–20.

25. Narayanan RM, Desetty MK, Reichenbach SE. Effect of spatial resolution on information content characterization in remote sensing imagery based on classification accuracy. Int J Remote Sens. 2010;23:537–53.

26. Fu B, Wang Y, Campbell A, Li Y, Zhang B, Yin S, et al. Comparison of object-based and pixel-based Random Forest algorithm for wetland vegetation mapping using high spatial resolution GF-1 and SAR data. Ecol Indic. 2017;73:105–17.

27. Mahdavi S, Salehi B, Amani M, Granger JE, Brisco B, Huang W, et al. Object-based classification of wetlands in Newfoundland and Labrador using multi-temporal PolSAR data. Can J Remote Sens. 2017;43:432–50.

28. De Luca G, Silva JMN, Cerasoli S, Araújo J, Campos J, Di Fazio S, et al. Object-based land cover classification of cork oak woodlands using UAV imagery and Orfeo ToolBox. Remote Sens. 2019;11:1238.

29. Duro DC, Franklin SE, Dubé MG. A comparison of pixel-based and object-based image analysis with selected machine learning algorithms for the classification of agricultural landscapes using SPOT-5 HRG imagery. Remote Sens Environ. 2012;118:259–72.

30. Pande-Chhetri R, Abd-Elrahman A, Liu T, Morton J, Wilhelm VL. Object-based classification of wetland vegetation using very high-resolution unmanned air system imagery. Eur J Remote Sens. 2017;50:564–76.

31. Geng R, Jin S, Fu B, Wang B. Object-based wetland classification using multi-feature combination of ultra-high spatial resolution multispectral images. Can J Remote Sens. 2021;46:784–802.

32. Fu B, Liu M, He H, Lan F, He X, Liu L, et al. Comparison of optimized object-based RF-DT algorithm and SegNet algorithm for classifying Karst wetland vegetation communities using ultra-high spatial resolution UAV data. Int J Appl Earth Obs Geoinf. 2021;104:102553.

33. Phantom 4 Pro/Pro_Plus Series User Manual CHS. https://dl.djicdn.com/downloads/phantom_4_pro/20211129/UM/Phantom_4_Pro_Pro_Plus_Series_User_Manual_CHS.pdf (accessed on 1 July 2022).

34. Cao J, Leng W, Liu K, Liu L, He Z, Zhu Y. Object-based mangrove species classification using unmanned aerial vehicle hyperspectral images and digital surface models. Remote Sens. 2018;10:89.

35. Akar A, Gökalp E, Akar Ö, Yılmaz V. Improving classification accuracy of spectrally similar land covers in the rangeland and plateau areas with a combination of WorldView-2 and UAV images. Geocarto Int. 2016;32:990–1003.

36. Qian Y, Zhou W, Yan J, Li W, Han L. Comparing machine learning classifiers for object-based land cover classification using very high resolution imagery. Remote Sens. 2014;7:153–68.

37. Drăguţ L, Tiede D, Levick SR. ESP: A tool to estimate scale parameter for multi-resolution image segmentation of remotely sensed data. Int J Geogr Inf Sci. 2010;24:859–71.

© 2025 The Author(s). | Published by Agro Intelligence Research Press

38. Michez A, Piegay H, Lisein J, Claessens H, Lejeune P. Classification of riparian forest species and health condition using multi-temporal and hyperspatial imagery from unmanned aerial system. Environ Monit Assess. 2016;188:146.

39. Meyer GE, Neto JC. Verification of color vegetation indices for automated crop imaging applications. Comput Electron Agric. 2008;63:282–93.

40. Lu B, He Y. Species classification using unmanned aerial vehicle (UAV)-acquired high spatial resolution imagery in a heterogeneous grassland. ISPRS J Photogramm Remote Sens. 2017;128:73–85.

41. Lou P, Fu B, He H, Li Y, Tang T, Lin X, et al. An optimized object-based Random Forest algorithm for marsh vegetation mapping using high-spatial-resolution GF-1 and ZY-3 data. Remote Sens. 2020;12:1270.

42. Ebrahimi-Khusfi Z, Nafarzadegan AR, Dargahian F. Predicting the number of dusty days around the desert wetlands in southeastern Iran using feature selection and machine learning techniques. Ecol Indic. 2021;125:107499.

43. Grabska E, Hostert P, Pflugmacher D, Ostapowicz K. Forest stand species mapping using the Sentinel-2 time series. Remote Sens. 2019;11:1197.

44. Dobrinić D, Gašparović M, Medak D. Sentinel-1 and 2 time-series for vegetation mapping using Random Forest classification: A case study of Northern Croatia. Remote Sens. 2021;13:2321.

45. Pham LTH, Brabyn L. Monitoring mangrove biomass change in Vietnam using SPOT images and an object-based approach combined with machine learning algorithms. ISPRS J Photogramm Remote Sens. 2017;128:86–97.

46. Pasquarella VJ, Holden CE, Woodcock CE. Improved mapping of forest type using spectral-temporal Landsat features. Remote Sens Environ. 2018;210:193–207.

47. Sun C, Li J, Liu Y, Liu Y, Liu R. Plant species classification in salt marshes using phenological parameters derived from Sentinel-2 pixel-differential time-series. Remote Sens Environ. 2021;256:112320.

48. Adugna T, Xu W, Fan J. Comparison of Random Forest and Support Vector Machine classifiers for regional land cover mapping using coarse resolution FY-3C images. Remote Sens. 2022;14:574.

49. Belgiu M, Drăguţ L. Random forest in remote sensing: A review of applications and future directions. ISPRS J Photogramm Remote Sens. 2016;114:24–31.

50. Millard K, Richardson M. On the importance of training data sample selection in Random Forest image classification: A case study in peatland ecosystem mapping. Remote Sens. 2015;7:8489–515.

51. Mohammadimanesh F, Salehi B, Mahdianpari M, Motagh M, Brisco B. An efficient feature optimization for wetland mapping by synergistic use of SAR intensity, interferometry, and polarimetry data. Int J Appl Earth Obs Geoinf. 2018;73:450–62.

52. Chabalala Y, Adam E, Ali KA. Machine learning classification of fused Sentinel-1 and Sentinel-2 image data towards mapping fruit plantations in highly heterogenous landscapes. Remote Sens. 2022;14:2621.

53. Martínez Prentice R, Villoslada Peciña M, Ward RD, Bergamo TF, Joyce CB, Sepp K. Machine learning classification and accuracy assessment from high-resolution images of coastal wetlands. Remote Sens. 2021;13:3669.

54. Thanh Noi P, Kappas M. Comparison of Random Forest, k-Nearest Neighbor, and Support Vector Machine classifiers for land cover classification using Sentinel-2 imagery. Sensors. 2017;18:18.

55. Zhou R, Yang C, Li E, Cai X, Yang J, Xia Y. Object-based wetland vegetation classification using multi-feature selection of unoccupied aerial vehicle RGB imagery. Remote Sens. 2021;13:4910.

© 2025 The Author(s). | Published by Agro Intelligence Research Press

56. Löw F, Michel U, Dech S, Conrad C. Impact of feature selection on the accuracy and spatial uncertainty of per-field crop classification using Support Vector Machines. ISPRS J Photogramm Remote Sens. 2013;85:102–19.

57. Petropoulos GP, Kalaitzidis C, Prasad Vadrevu K. Support vector machines and object-based classification for obtaining land-use/cover cartography from Hyperion hyperspectral imagery. Comput Geosci. 2012;41:99–107.

58. Zhang X, Xu J, Chen Y, Xu K, Wang D. Coastal wetland classification with GF-3 polarimetric SAR imagery by using object-oriented Random Forest algorithm. Sensors. 2021;21:3395.

59. Tian Y, Jia M, Wang Z, Mao D, Du B, Wang C. Monitoring invasion process of Spartina alterniflora by seasonal Sentinel-2 imagery and an object-based Random Forest classification. Remote Sens. 2020;12:1383.

60. Ma L, Cheng L, Li M, Liu Y, Ma X. Training set size, scale, and features in Geographic Object-Based Image Analysis of very high resolution unmanned aerial vehicle imagery. ISPRS J Photogramm Remote Sens. 2015;102:14–27.

61. Schaaf AN, Dennison PE, Fryer GK, Roth KL, Roberts DA. Mapping plant functional types at multiple spatial resolutions using imaging spectrometer data. GIScience Remote Sens. 2013;48:324–44.

62. Zhao L, Shi Y, Liu B, Hovis C, Duan Y, Shi Z. Finer classification of crops by fusing UAV images and Sentinel-2A data. Remote Sens. 2019;11:3012.

63. Peña MA, Cruz P, Roig M. The effect of spectral and spatial degradation of hyperspectral imagery for the Sclerophyll tree species classification. Int J Remote Sens. 2013;34:7113–30.

64. Villoslada M, Bergamo TF, Ward RD, Burnside NG, Joyce CB, Bunce RGH, et al. Fine scale plant community assessment in coastal meadows using UAV based multispectral data. Ecol Indic. 2020;111:105979.

65. Underwood EC, Ustin SL, Ramirez CM. A comparison of spatial and spectral image resolution for mapping invasive plants in coastal California. Environ Manag. 2007;39:63–83.

© 2025 The Author(s). | Published by Agro Intelligence Research Press